Supplement of Earth Surf. Dynam., 6, 989–1010, 2018
https://doi.org/10.5194/esurf-6-989-2018-supplement

Earth Surface Dynamics
Open Access
EGU

Supplement of

Morphodynamic model of the lower Yellow River: flux or entrainment form for sediment mass conservation?

Chenge An et al.

Correspondence to: Chenge An (anchenge08@163.com) and Xudong Fu (xdfu@tsinghua.edu.cn)

S1: Comparison of two relations for sediment fall velocity: Dietrich (1982) against Ferguson and Church (2004)

In this paper, we implement the relation of Dietrich (1982) to calculate sediment fall velocity v_s. The relation is,

$$v_s = R_f \sqrt{RgD} \tag{S1}$$

$$\ell n\left(R_f\right) = -b_1 + b_2 \ell n\left(\mathrm{Re}_p\right) - b_3\left[\ell n\left(\mathrm{Re}_p\right)\right]^2 - b_4\left[\ell n\left(\mathrm{Re}_p\right)\right]^3 + b_5\left[\ell n\left(\mathrm{Re}_p\right)\right]^4 \tag{S2}$$

$$\mathrm{Re}_p = \frac{\sqrt{RgD}D}{\nu} \tag{S3}$$

where b_1 = 2.891394, b_2 = 0.95296, b_3 = 0.056835, b_4 = 0.002892, b_5 = 0.000245, and $\nu = 10^{-6}$ is the kinematic viscosity of water.

Another widely used relation for sediment fall velocity is the relation of Ferguson and Church (2004), which is regarded as applying to nearly the entire range of viscous to turbulent conditions.

$$v_s = \frac{RgD^2}{C_1\nu + \left(0.75C_2RgD^3\right)^{0.5}} \tag{S4}$$

where C_1 = 18 and C_2 = 0.4 for smooth spheres; C_1 = 18 and C_2 = 1.0 for sieve diameters of natural sand; and C_1 = 20 and C_2 = 1.1 for nominal diameters of natural sand. More specifically, the relation of Ferguson and Church (2004) converges to Stokes' law for small grains, and to a constant drag coefficient for large grains.

Considering the fact that the sediment of LYR is finer than most sand-bed rivers (Ma et al., 2017), here we compare the two relations for sediment fall velocity in the context of the LYR. The two parameters in Ferguson and Church are specified as C_1 = 18 and C_2 = 1.0. In our simulation, the sediment size range of the LYR is specified as 15 μm ~ 500 μm.

According to Fig. S1, the relation of Dietrich (1982) and the relation of Ferguson and Church (2004) coincide with each other within this size range, thus justifying our implementation of Dietrich (1982) in the simulation. For grain sizes smaller than 15 μm, sediment becomes washload in the LYR and Dietrich (1982) predicts sediment fall velocities that are smaller than those predicted by Ferguson and Church (2004). For sediment coarser than 500 μm, Dietrich (1982) somewhat overestimates sediment fall velocity compared with Ferguson and Church (2004).

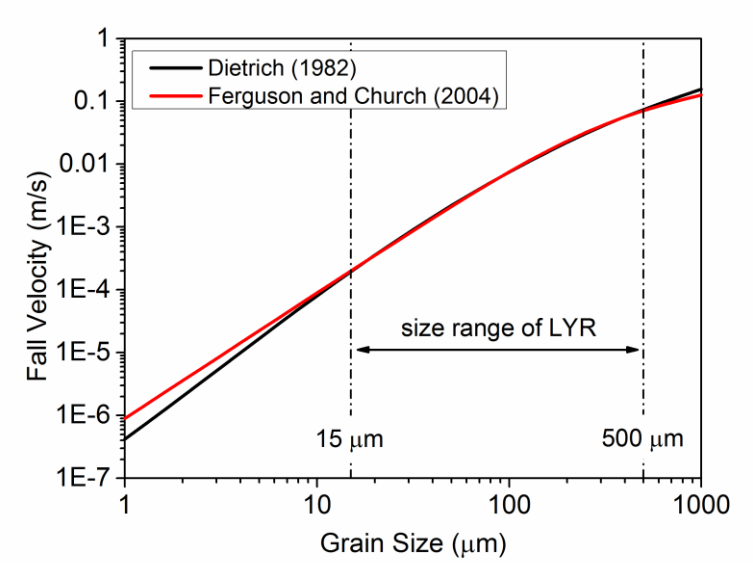

Figure S1. Comparison of two relations for sediment fall velocity: Dietrich (1982) and Ferguson and Church (2004)

S2: Numerical simulation of uniform sediment under hydrographs

In this section, we conduct additional cases for the case of uniform sediment. The computational conditions are the same as those implemented in Section 3.1 of the main text, except that the unsteady inflow discharge is considered. The flood has a symmetrical triangular hydrograph with a peak discharge of 3000 m^3/s (corresponding to a discharge per unit width of 10 m^2/s), a minimum discharge of 300 m^3/s (corresponding to a discharge per unit width of 1 m^2/s), and a flood duration of 4 days. Figure S2 shows the hydrograph as used here. The flood intermittency factor is specified as unity since hydrographs are being considered. The sediment supply rate is the same as that in Section 3.1 of the main text, thus corresponding to a cutoff of sediment supply. The hydrograph is repeated for 3 times.

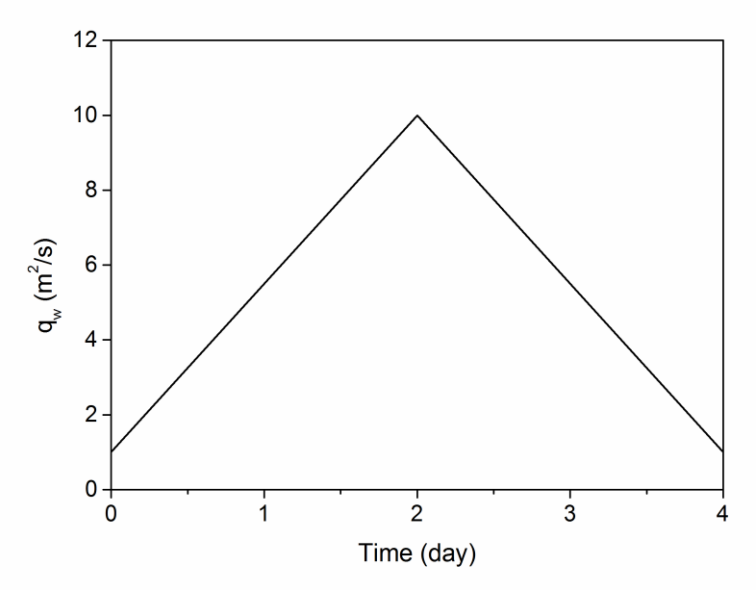

Figure S2. Hydrograph of the inflow discharge

Figure S3 shows the river evolution within the 3 floods predicted by the flux form of Exner equation. Due to the cutoff of sediment supply, the bed degrades and the sediment load declines from the upstream end. Moreover, sediment load shows a reduction in the downstream direction at the peak discharge, but an increase at the low discharge, which corresponds to the nonuniformity of the flow hydraulics (i.e. the propagation of a flood wave). Figure S4 shows the river evolution predicted by the entrainment form of the Exner equation, with the sediment fall velocity calculated by the relation of Dietrich (1982). A comparison of Figs. S3 and S4 indicates that the two formulations predict very similar results even when hydrographs are considered.

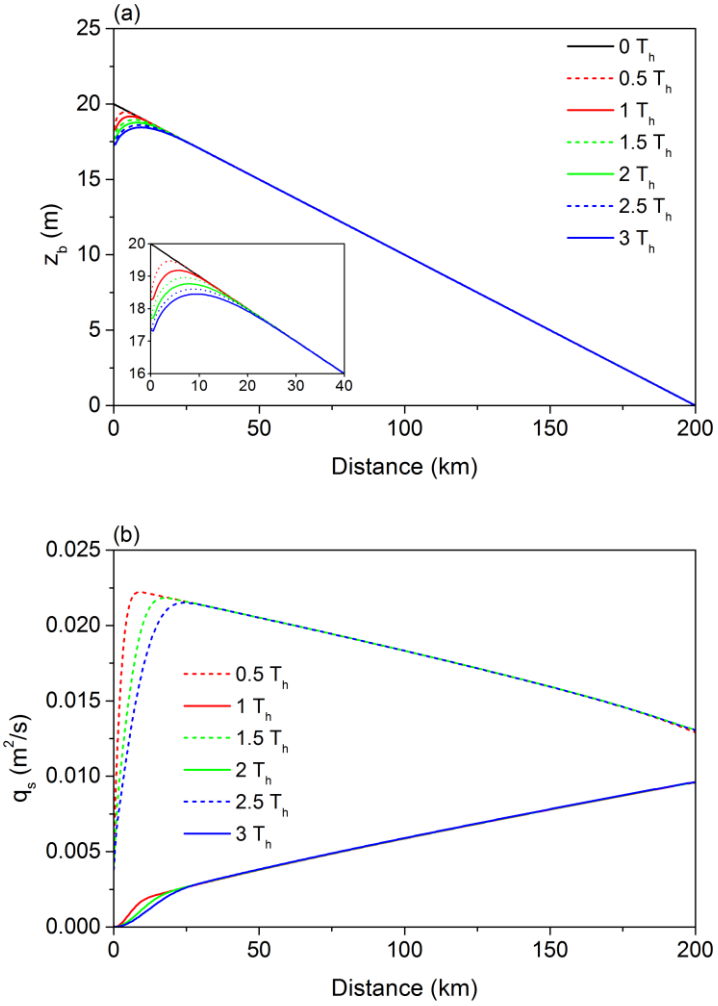

Figure S3. Results for uniform sediment within 3 hydrographs simulated by the flux form of Exner equation: time variation of (a) bed elevation z_b, (b) sediment load per unit width q_s of the LYR in response to the cutoff of sediment supply. The inset shows detailed results near the upstream end. The dash lines are at the peak discharge and the solid lines are at the minimum discharge.

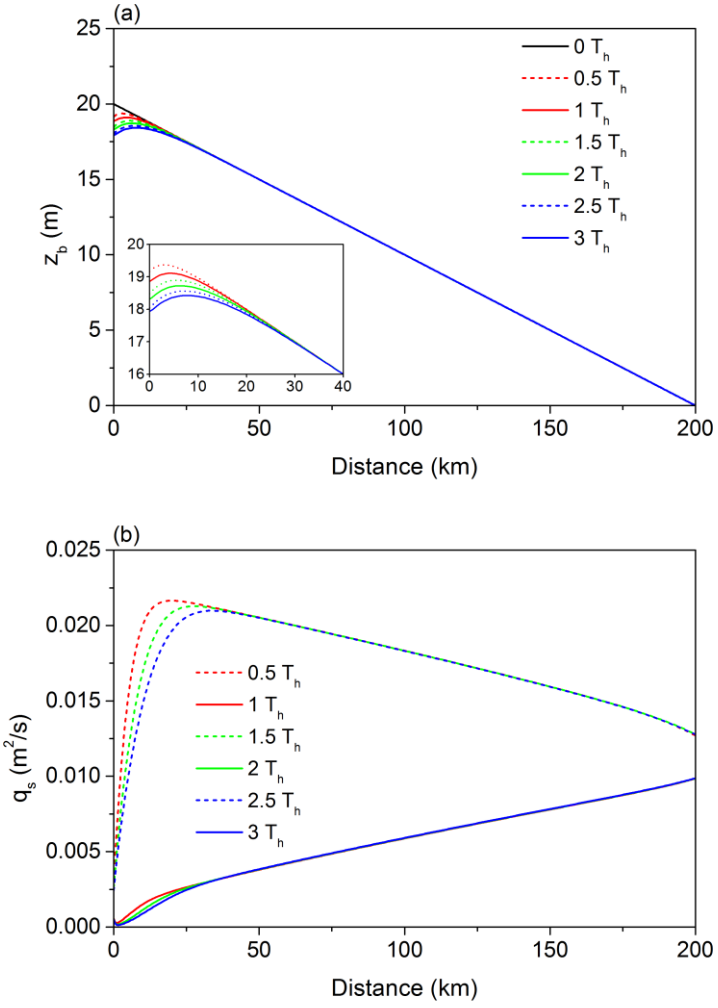

Figure S4. Results for uniform sediment within 3 hydrographs simulated by the entrainment form of Exner equation: time variation of (a) bed elevation z_b, (b) sediment load per unit width q_s of the LYR in response to the cutoff of sediment supply. The inset shows detailed results near the upstream end. The dash lines are at the peak discharge and the solid lines are at the minimum discharge.

S3: Numerical simulation of sediment mixtures under hydrographs

In this section, we study additional examples for the case of sediment mixtures. The computational conditions are the same as those implemented in Section 3.2 of the main text, except that the unsteady inflow discharge is considered. The flood

hydrograph is identical to that in Section S2, as shown in Fig. S2. The sediment supply rate is the same as that in Section 3.2 of the main text, thus corresponding to a cutoff of sediment supply. The hydrograph is repeated for 3 times.

Figure S5 shows the river evolution within the first 3 floods predicted by the flux form of Exner equation, and Fig. S6 shows the river evolution predicted by the entrainment form of Exner equation. The sediment fall velocity is calculated by the relation of Dietrich (1982). Even though the river morphodynamic processes become much more complicated when the hydrograph rather than constant flow discharge is considered, a comparison of Figs. S5 and S6 still shows that the two formulations predict very different patterns of grain sorting. Kinematic waves are evident in the flux form, but no kinematic waves are evident in the entrainment form.

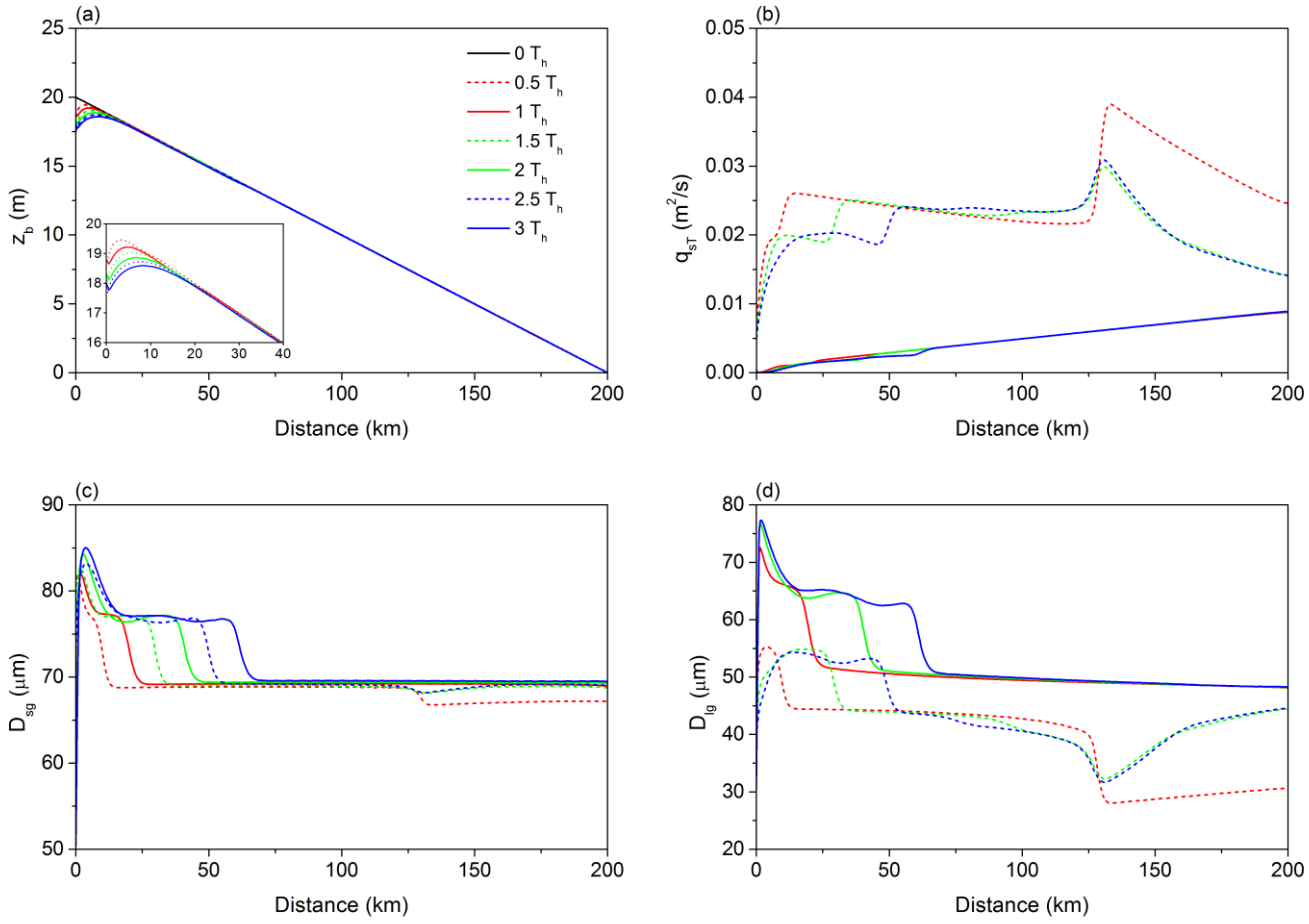

Figure S5. Results for sediment mixtures within 3 hydrographs simulated by the flux form of Exner equation: time variation of (a) bed elevation z_b, (b) total sediment load q_{sT}, (c) surface geometric mean grain size D_{sg} and (d) geometric mean grain size

of sediment load of the LYR in response to the cutoff of sediment supply. The inset shows detailed results near the upstream end. The dash lines are at the peak discharge and the solid lines are at the minimum discharge.

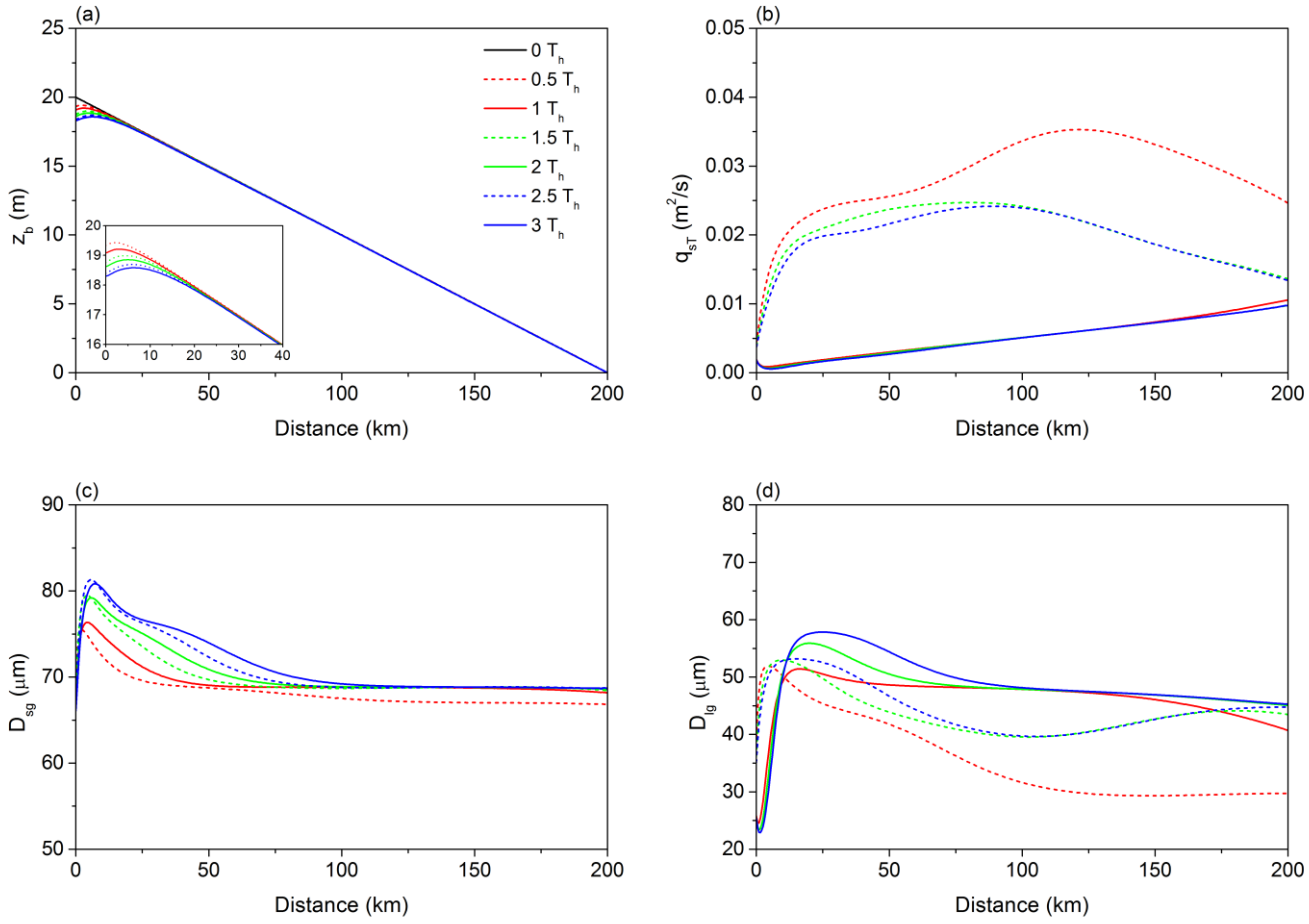

Figure S6. Results for sediment mixtures within 3 hydrographs simulated by the entrainment form of Exner equation: time variation of (a) bed elevation z_b, (b) total sediment load q_{sT}, (c) surface geometric mean grain size D_{sg} and (d) geometric mean grain size of sediment load of the LYR in response to the cutoff of sediment supply. The inset shows detailed results near the upstream end. The dash lines are at the peak discharge and the solid lines are at the minimum discharge.

S4: Iterative solution of sediment transport rate q_{si} in the entrainment form

The parameter q_{si} in Eq. (40) of the main text is solved iteratively as given below,

$$q_{si}^{(m+1)} = q_{sei} - \frac{q_w}{v_{si} r_{oi}} \left[\frac{1}{I_f} \frac{\partial \left(\frac{q_{si}^{(m)}}{u} \right)}{\partial t} + \frac{\partial q_{si}^{(m)}}{\partial x} \right] \tag{S5}$$

where the superscript denotes the order of iteration. The following zero-order solution is specified as an initial value;

$$q_{si}^{(0)} = q_{sei} \tag{S6}$$

From this we can get the first order and second order solutions,

$$q_{si}^{(1)} = q_{sei} - \frac{q_w}{v_{si} r_{oi}} \left[\frac{1}{I_f} \frac{\partial \left(\frac{q_{sei}}{u} \right)}{\partial t} + \frac{\partial q_{sei}}{\partial x} \right] \tag{S7}$$

$$q_{si}^{(2)} = q_{sei} - \frac{q_w}{v_{si} r_{oi}} \frac{1}{I_f} \frac{\partial}{\partial t} \frac{1}{u} \left\{ q_{sei} - \frac{q_w}{v_{si} r_{oi}} \left[\frac{1}{I_f} \frac{\partial \left(\frac{q_{sei}}{u} \right)}{\partial t} + \frac{\partial q_{sei}}{\partial x} \right] \right\} - \frac{q_w}{v_{si} r_{oi}} \frac{\partial}{\partial x} \left\{ q_{sei} - \frac{q_w}{v_{si} r_{oi}} \left[\frac{1}{I_f} \frac{\partial \left(\frac{q_{sei}}{u} \right)}{\partial t} + \frac{\partial q_{sei}}{\partial x} \right] \right\} \tag{S8}$$

The second order iterative solution to Eq. (S8) is tedious in form, but the only terms of importance on the right-hand side are the spatial derivatives. Therefore we drop the time derivatives for simplicity. This gives,

$$q_{si} = q_{sei} - \frac{q_w}{v_{si} r_{oi}} \frac{\partial}{\partial x} \left(q_{sei} - \frac{q_w}{v_{si} r_{oi}} \frac{\partial q_{sei}}{\partial x} \right) \tag{S9}$$

which corresponds to Eq. (41) as implemented in Section 4.2 of the main text.